DETERMINING THE STRAIN RATE DEPENDENCE OF CORTICAL AND CANCELLOUS BONES OF HUMAN TIBIA USING A SPLIT HOPKINSON PRESSURE BAR

A.Chawla[1], S.Mukherjee, Ch.Kranthi Teja

Indian Institute of Technology, Delhi.

ABSTRACT:

Mechanical properties of tibial bone at compressive strain rates of 50-200 /s are obtained through Split Hopkinson pressure bar. Cylindrical specimens of 12-15 mm diameter and 2-5 mm thickness were prepared. The Young's moduli are calculated from linear portion of stress-strain curves. For both cortical and cancellous part of the bones, the Young's modulus was found to increase with the increasing strain rates. Also for both cancellous and cortical bones the Young's modulus increases consistently with increase in densities.

Keywords: Split Hopkinson pressure bar, Young's modulus, apparent density, cancellous bone, cortical bone and strain rate.

INTRODUCTION:

Safety measures have traditionally been evaluated by full-scale crash testing. The high cost and that it can be conducted only after a prototype is available has been a barrier in investigating alternatives for limiting injuries. Computer simulations are cost effective as compared to full-scale

[1] Corresponding Author, achawla64@gmail.com, Tel: +91-11-26591058, Fax: +91-11-26582053

crash tests, and also provide a great deal of information that is frequently unavailable from full-scale crash testing. Unlike full-scale crash tests that normally yield data for only predetermined points where sensors have been mounted, computer simulations can be used to identify all areas where a design needs additional reinforcement or areas where a component has excess capacity. For example, finite element modeling provides designers with an accurate picture of the stress distributions in critical components of a safety device throughout the impact event. After a computer simulation has been developed and successfully validated against full-scale crash tests, the cost associated with conducting parametric studies to investigate the effects of installation details, impact conditions, road furniture, and vehicle characteristics is relatively inexpensive (Shima et al., 2005).

Computer simulations of vehicle collisions have improved significantly over the past few years. With advances in computer technology and non-linear finite element (FE) codes, full scale models and simulations of sophisticated phenomena like in biological systems are becoming ever more possible. Finite element crash simulations have been primarily focused on the vehicle models and their crash characteristics. Recently, refined FE models of airbags and dummies have been added to the simulations. This allows assessment of occupant injury and restraint system performance. Specifically, a well-developed human body model helps in understanding injury mechanisms and also helps to know the effect of modifications made to vehicles.

Efficient human body model development requires detailed modeling of the geometry of the human body and extensive tissue and bone properties beyond those already available in literature, such as dynamic properties of bones. Compressive mechanical properties of Tibial bones at strain rates and loading direction transverse to the length of the bone as expected in automotive related crashes are reported here.

Knee injuries occur most commonly in frontal and side crashes. Most of these are due to direct impact with the knee bolster, dashboard, steering wheel and console or side door structures and there are evidences that the anterior superior tibial region is contused (Nordhoff, 2005). Table 8 shows the injury risk and odds ratios for lower extremity sub-regions of occupants in frontal crashes, highlighting the importance of lower extremities.

Table 1: is to be inserted here.

(Rudd, 2009) characterized the dynamic compressive mechanical properties of cancellous bone from the human cervical spine using SHPB. The static and dynamic compressive responses of cancellous bone specimens from the human cervical spine were studied experimentally.

(Ferreira et al., 2004) characterized the mechanical properties of bovine cortical bone at high strain rate using SHPB. The study evidenced that bone is a highly heterogeneous structure and scattering of results is significant. It was observed that for an increase of strain rate the resistance properties increased and stiffness properties decreased.

(Westhuizen et al., 2007) characterized the strain rate dependent mechanical properties of bovine bone in axial compression by quasi-static and dynamic tests.

This work reports the Young's modulus of cancellous and cortical human bones from the tibia at varying strain rates and density. To account for the scatter, design of experiments techniques are used to come to conclusion regarding the trends.

SPLIT HOPKINSON PRESSURE BAR:

The SHPB, schematically shown in

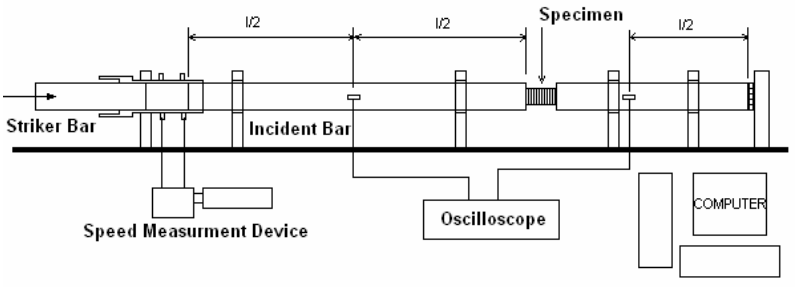

Figure 1 is one of the most widely accepted tests for characterizing materials at large strain rates. A striker impacts the incident bar; setting up a traveling longitudinal strain wave which is tracked by strain gauging. A specimen is introduced in between the incident bar and reflecting bar. The stiffness characteristics of the specimen attenuate the wave transmission, modifying the pulse transmitted to the reflecting bar and reflected back from the interface to the incident bar.

Figure 1: is to be inserted here

Typically, the incident and reflecting bar are selected in such a manner that the impedance of the bar is of the same order as the impedance of the material to be tested. The bars for testing cancellous bones are made of PTFE (Poly Tetra Fluoro Ethylene) and for testing cortical bones are made of Aluminium. In the PTFE bars there is significant attenuation and dispersion of the wave as it propagates. The attenuation is characterized by using the experimental procedure established by Bacon and Brun. Then the pulses are reconstructed at the bar-specimen interface by compensating for the decay (Chawla et al., 2006).

CONVENTIONAL SPLIT HOPKINSON PRESSURE BAR ANALYSIS:

For SHPB with a conventional (elastic) material it is assumed that the stress acting on each cross-sectional area of the bar is uniform, the bar is stressed within the elastic limit, and attenuation

and dispersion are negligible and that the specimen remains in equilibrium throughout the test. With these assumptions the equilibrium of an element of length δx (

Figure 2) gives the following relation:

$$\frac{\partial^2 u}{\partial t^2} = c_0{}^2 \frac{\partial^2 u}{\partial x^2} \text{ Where } C_0 = \frac{E}{\rho} \qquad (1)$$

Figure 1: is to be inserted here.

The solution of this equation may be written as:

$$u = f(c_0 t - x) + F(c_0 t + x) \qquad (2) \qquad (2.1)$$

Where *f* and *F* are arbitrary functions and depend on the initial conditions. Considering the wave traveling in the direction of decreasing *x*,

$$u = f(c_0 t + x) \qquad (3)$$

From this, $\frac{\partial u}{\partial t} = C_0 \frac{\partial u}{\partial x}$ and since $\frac{\partial u}{\partial x} = \frac{\sigma_{xx}}{E}$,

$$\sigma_{xx} = \rho C_0 \frac{\partial u}{\partial t} \qquad (4)$$

This shows that there is a linear relationship between stress at any point and particle velocity. The quantity ρC_0 is called as characteristic impedance and is defined as the ratio of force to particle velocity (Graff, 1991).

Considering the wave traveling in both direction of '*x*' after subsequent reflection from the end of the bars, the particle displacement in the striker and incident bars, can be written as:

$$u_s = f_s(c_0 t - x) + F_s(c_0 t + x) \qquad (5)$$

$$u_i = f_i(c_0 t - x) + F_i(c_0 t + x) \qquad (6)$$

Differentiating and using the initial conditions and known bar properties in this case, it can be shown that (Graff, 1991)

$$f_s' = -F_s' = \frac{-V_s}{2C_0} \text{ and } f_i' = F_i' = 0 \qquad (7)$$

The length of the pulse, l_p is $2l_s$ and the duration of the pulse, T is $\frac{2l_s}{c_0}$

The average stress in the specimen can be related to the forces exerted on each face of the specimen.

Figure 3 shows a cylindrical specimen subjected to forces exerted by the input and output bars.

Figure 3: is to be inserted here.

The forces at the end of the pressure bars may be expressed in terms of the incident and reflected pressure bar strains and the average stress can be calculated as

$$\sigma_{avg}(t) = \frac{E d_{bar}^{\ 2}}{2 d_{sp}^{\ 2}} [\varepsilon_i(t) + \varepsilon_r(t) + \varepsilon_t(t)] \qquad (8) \qquad (2.2)$$

Where d_{bar}, and d_{sp} are the diameters of the bar and the specimen respectively and the subscripts i, r and t refer to the incident, reflected and transmitted pulses.

Thus the average stress in the specimen can be calculated by measuring $\varepsilon_i(t)$, $\varepsilon_r(t)$ and $\varepsilon_t(t)$ using strain gauges mounted on the respective bar. The strain rate at a uniform rate of straining is defined as strain divided by time over which the straining occurs. Therefore, strain rate in deforming specimen is given by:

$$\frac{d\varepsilon}{dt} = \frac{v_1 - v_2}{l_{sp}} = \frac{c_0}{l_{sp}}[\varepsilon_i(t) - \varepsilon_r(t) - \varepsilon_t(t)] \qquad (9)$$

The total strain can be calculated by integrating the above equation over the duration of the pulse. A simpler expression using only the reflected and transmitted pulse is used often under the assumption that dynamic balance is achieved in the specimen. We found that dynamic balance is not achieved and so retained the form presented here.

The most common way to display the results is in a dynamic stress–strain diagram. This diagram exhibits different curves at growing strain rates.

MATERIALS AND METHODS:

For cancellous bone the impedance is around 40 kg/s. So for characterizing the dynamic properties of these bones PTFE bars are chosen. For cortical bone the impedance is around 500 kg/s. So for characterizing dynamic properties of these bones Aluminum bars are chosen.

The overall dimensions of the test rig shown in

Figure 4 are 2.5m × 0.2m × 0.15m. This includes two PTFE or Al bars as incident and transmitted bars each of 1m length and 10 mm diameter, two striker bars (PTFE, Al) with length 1m

and diameter 10mm. The striker bar is launched from a spring loaded gun. An infrared source and receiver system is used for velocity measurement.

Foil type strain gauges with active length 1.5mm and resistance of 350 ohms are used. VISHAY 2310B signal conditioning amplifier is used and an excitation voltage of 5 V is applied across the Wheatstone bridge. An Agilent 54621A oscilloscope was used for recording the time history of the bridge output voltages. It is capable of sampling at 60 MHZ with two different input channels one for incident bar and one for transmitted bar. Data can be transferred from the oscilloscope to computer for further processing using a floppy disk.

Figure 4: is to be inserted here.

A set of 36 specimens of cortical bones and 12 specimens of cancellous bones are prepared from human tibia. All the cortical bones are prepared along the radial direction of tibia, 10 cancellous bone specimens are prepared along the length of the tibia and only 2 specimens are prepared along the radial direction of tibia. The specimens were machined to a disk shape (with length of 2-4 mm and diameter of 12 mm) as shown in

Figure 5. The bone specimens are sandwiched between incident and transmitted bars as shown in 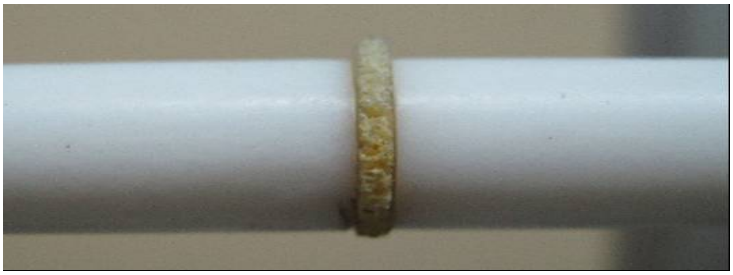

Figure 6 and all the tests are performed at room temperature of 25^{o}C. Then post processing of experimental data was performed.

Figure 5: is to be inserted here.

Figure 6: is to be inserted here.

Typical strain pulses are shown in Figure 8 for cancellous and in

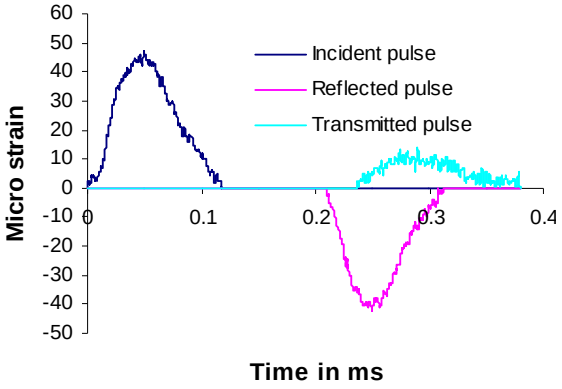

Figure 9 for cortical bones. The peak strains are of the same order and we found that the transmitted pulse consistently lags the reflected pulse.

Figure 7: is to be inserted here.

Figure 8: is to be inserted here.

Figure 9: is to be inserted here.

Figure 10: is to be inserted here.Error! Not a valid bookmark self-reference. & Figure 11 show typical stress-strain response for the cancellous and cortical bones. The constant strain rate is identified from the strain vs. time history as shown in Figure 7. The stress-strain response is plotted for this constant strain rate portion. Hence the reported stress and strain values start from non-zero values : Typical Stress-strain response for cancellous bones

Figure 11: is to be inserted here.

RESULTS AND DISCUSSION:

The tests are categorized as series S1-S4 based on density for cancellous bones and S5-S16 for cortical bones. Each series was tested at three different strain rates. Then Young's modulus of bone was determined for both cancellous and cortical bones by estimating slope of the stress-strain

curves upto 0.1% strain for cortical and 1% strain for cancellous bones as shown in

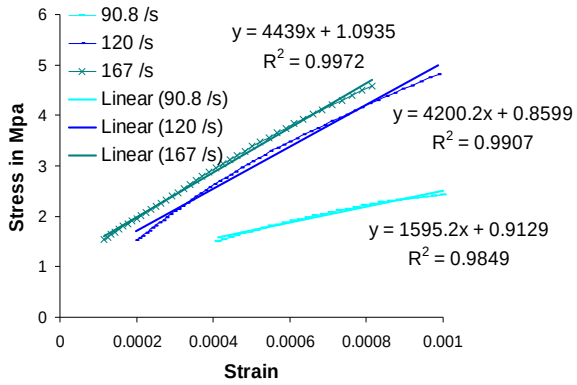

Figure 12. Young's modulus is identified to be 1.6, 4.2 and 4.5 GPa for strain rates 90.8, 120 and 167 /s respectively.

Figure 12: is to be inserted here.

Only two cancellous bone specimens 1S23 and 2S16 were prepared from the radial direction of tibia and all the remaining specimens along the longitudinal direction of tibia. It was observed that the Young's modulus of the specimens prepared from radial direction was larger compared to that along the longitudinal direction. From each series it was observed that the Young's modulus of cancellous bone increased with increase in strain rate.

Table 2: is to be inserted here.

Table 3: is to be inserted here.

All the cortical bones specimens are prepared from the radial direction of human tibia. Increase in Young's modulus with increase in strain rate is also observed for cortical bone.

To quantify Young's modulus variation with respect to density and strain rate, Taguchi method was applied. Orthogonal sets are identified for the cancellous bones from the experimental set shown in Table 9. Three levels are chosen on strain rate namely 120, 165, 200 /s and four levels are chosen on the density 800, 885, 1000 and 1175 kg/m^3 as shown in Table 11. The size is $3^5 \times 6^1$.

Table 4: is to be inserted here.

Ai represents average modulus for ith density at all the strain rate levels. Similarly *Bi* represents average modulus for ith Strain rate at all the density levels. The results of the effect of each factor level on Young's modulus of bone are shown in Table 12.

Table 5: is be inserted here.

Figure 13: is to be inserted here.

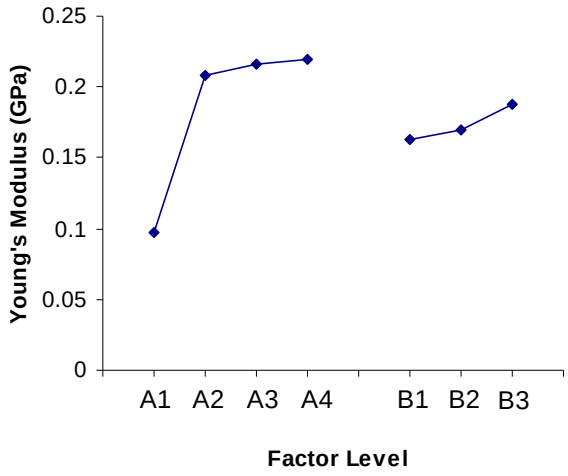

Figure **13**, indicates that the Young's modulus of bone increases with increase in strain rate. Also that the Young's modulus of bone increases with increase in density of cancellous bone. For strain rate variation of 120-200 /s the Young's modulus of bone observed to increase from 0.16-0.19 GPa. For density variation of 800-1175 Kg/m^3 the Young's modulus increases from 0.1-0.22 GPa.

Orthogonal sets are identified for the cortical bones in the experimental set shown in Table 10. Three levels are chosen on strain rate namely 65, 105, 145 /s and twelve levels are chosen on the density 1380, 1450, 1560, 1585, 1595, 1615, 1645, 1655, 1700, 1775, 1795 and 1850 kg/m^3 as shown in Table 13. The size is $3^{12} \times 12^1$.

Table 6: **is to be inserted here**.

The results of the effect of each factor level on Young's modulus of bone are shown in Table

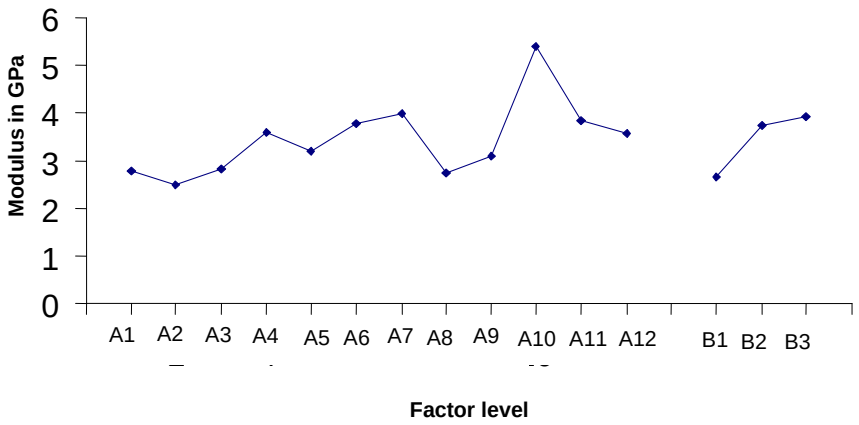

14. We infer from

Figure **14** which plots the factor level and the modulus that with increase in strain rate the Young's modulus of bone increases. Further, with increase in density of cortical bone, the Young's modulus of bone increases except at density levels of A11 and A12. For strain rate variation of 60-150 /s the Young's modulus of the cortical bone was observed to increase from 2.66-3.92 GPa. For density variation of 1380-1775 Kg/m^3 the Young's modulus of cortical bone increased from 2.8-5.4 GPa. Overall for the density variation of 800-1775 Kg/m^3 the Young's modulus of bone varies from 0.06-6.4 GPa.

Table 7: to be inserted here.

Figure 14: is to be inserted here.

CONCLUSIONS

The stress strain characterization of elastic modulus of both cancellous and cortical bone specimens has been conducted at varying rates. The geometrical accuracy of the machined

specimens has a bearing on the final strain rate achieved. The technique is suitable to determine mechanical properties of cancellous and cortical bones at high strain rates.

The spread of the data is consistent with the highly heterogeneous structure of bones. With increase in strain rate and density, the stiffness properties of both cortical and cancellous bones increased. It was also observed that the specimens from radial direction are stiffer than those from longitudinal direction of the human tibia.

REFERENCES:

1. Chawla A, Mukherjee S, Marathe R, Karthikeyan B (IIT, Delhi) Malhotra R (AIIMS, Delhi), (2006),"Determining strain rate dependence of human body soft tissues using a split hopkinson pressure bar", IRCOBI Conference, 2006.
2. Ferreira F, Vaz MA, Simoes JA, (2004), "Mechanical properties of bovine cortical bone at high strain rate", Materials Science & Technology, vol. 16, pp. 17-23, 2004.
3. Graff, K.F., (1991), "Wave Motion in Elastic Solids", Dover, New York, 1991.
4. Nordhoff L. S., (2005), "Motor vehicle collision injuries", Jones & Bartlett, 2005.
5. Rudd R W, (2009), "Updated analysis of lower extremity injury risk in frontal crashes in united states", National Highway Traffic Safety Administration, United States, Paper Number 09-0556, 2009.
6. Shima V.P.W., Yanga L.M., Liua J.F., Leeb V.S., (2005), "Characterisation of the dynamic compressive mechanical properties of cancellous bone from the human cervical spine". International Journal of Impact Engineering, Volume 32, Issues 1-4, Pages 525-540, 2005.
7. Westhuizen V.D., cloete T.J., Kok S., Nurick G.N., (2007), "Strain rate dependent mechanical properties of bovine bone in axial compression", **I**RCOBI Conference, 2007.

List of Figures

List of tables

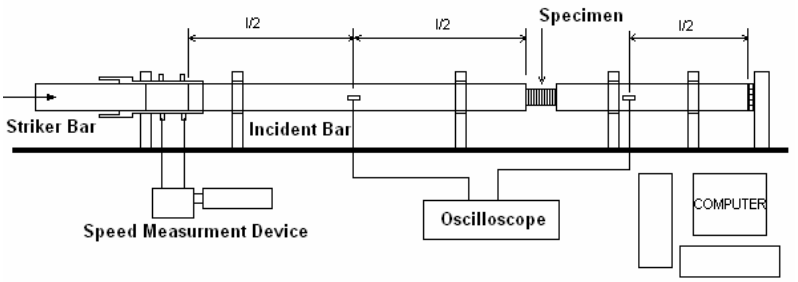

Figure 1: SHPB SCHEMATIC (Ferreira et al., 2004)

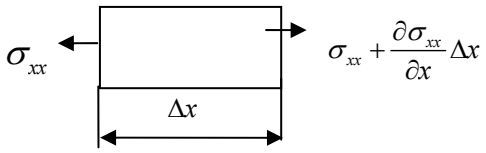

Figure 2: Schematic of an element in SHPB

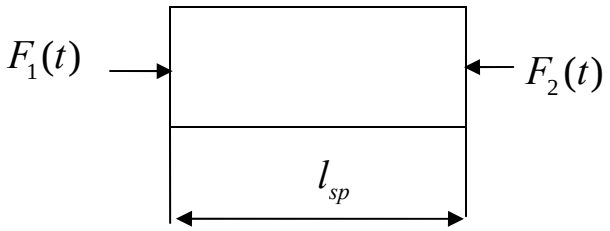

Figure 3: schematic of cylindrical specimen

Figure 4: SHPB setup using PTFE bars

Figure 5: Specimens after machining

Figure 6: Bone specimen after mounting

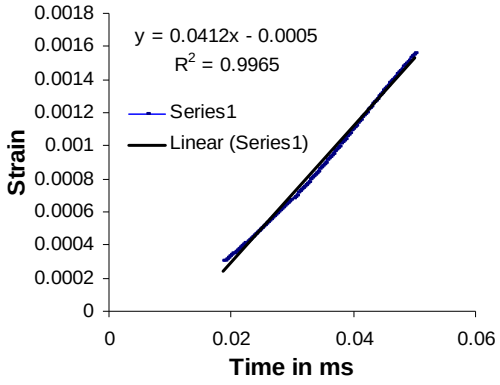

Figure 7: Identification of constant strain rate from strain-time history

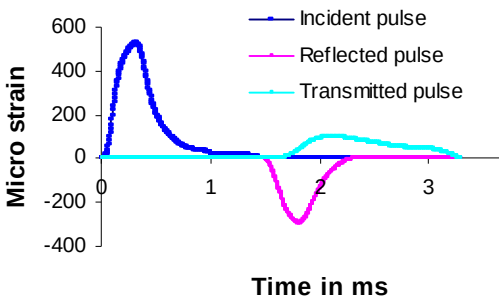

Figure 8: Typical strain pulses for cancellous bones using PTFE bars.

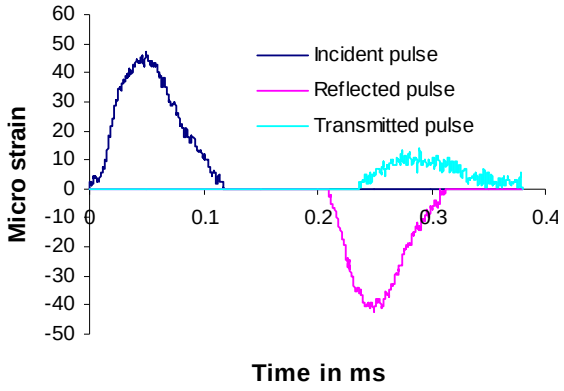

Figure 9: Typical Strain pulses for cortical bones using Al bars.

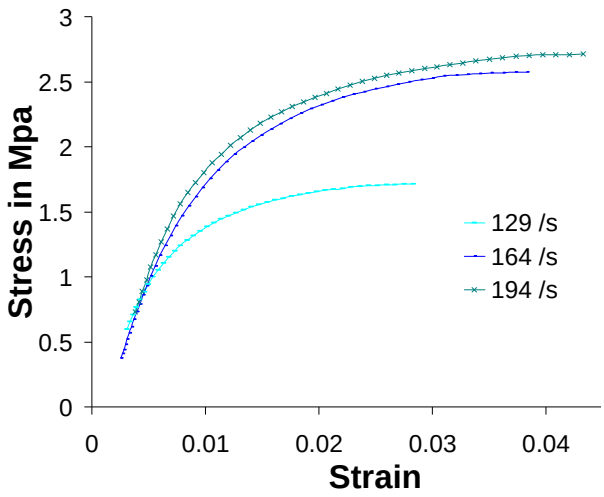

Figure 10: Typical Stress-strain response for cancellous bones.

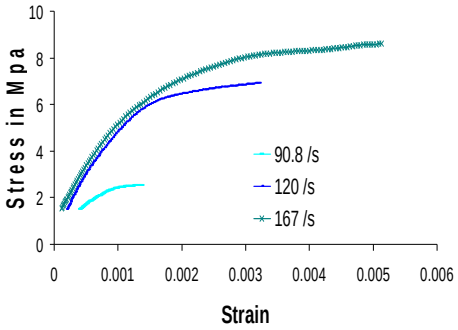

Figure 11: Typical Stress-strain response for cortical bones

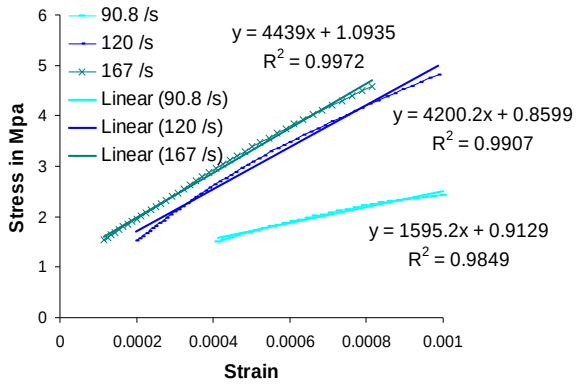

Figure 12: Determination of Young's modulus for cortical bones

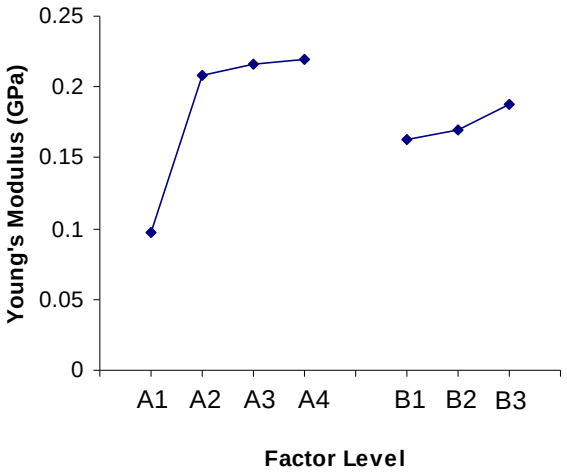

Figure 13: Effect of density and strain rate on Young's modulus of the bone

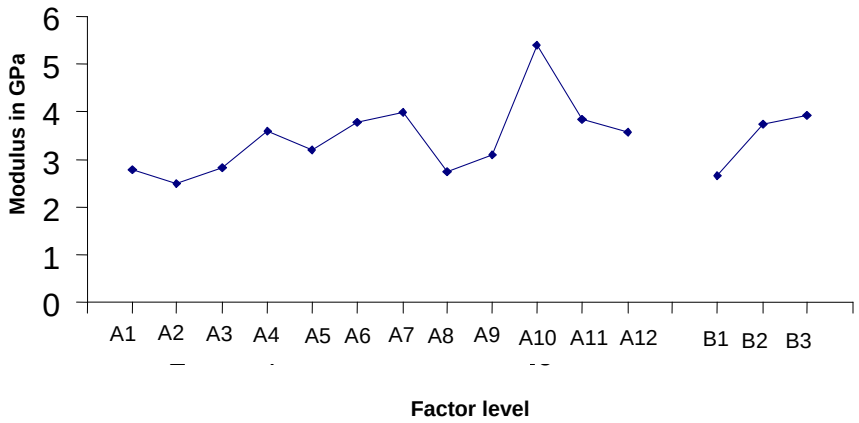

Figure 14: Effect of density and strain rate on Young's modulus of the bone

Table 8: Injury risk (AIS 2+) and odds ratios for lower extremity sub-regions of drivers (Shima et al., 2005)

CRASH TYPE	PELVIS	HIP	THIGH	KNEE	LEG	FOOT/ANKLE
Full Frontal	0.5%	0.14%	0.37%	0.63%	0.65%	2.12%
Left Offset	0.28%	0.19%	0.29%	0.48%	0.78%	1.26%
Right Offset	0.2%	0.14%	0.27%	0.52%	0.42%	1.06%

Table 9: Stiffness properties of cancellous bones

Series	Specimen Number	Density in kg/m^3	Strain rate /s	Young's Modulus GPa
S1	1S23	810	156	0.174
	T11	776	180	0.059
	T3	811	216	0.099
S2	T15	887	85	0.117

Table 10: Stiffness properties of cortical bones

Z	Specimen Number	Density in kg/m^3	Strain rate /s	Young's Modulus GPa
S5	2S22	1385	68.8	2.57
	2S10	1383	93.9	3.2
	1S9	1369	127	2.608
S6	1S6	1461	64	1.7
	1S17	1456	115	2.43
	1S19	1440	186	3.3
S7	2S24	1555	60	2.2
	1S26	1560	105	2.93
	2S8	1573	137.4	3.3
S8	1S13	1587	92	3.7
	1S25	1582	117	4.1
	2S25	1590	133	2.96
S9	1S14	1593	41.2	1.44
	1S12	1595	99.73	4.53
	1S18	1603	132	3.62
S10	2S2	1605	68.5	3.31
	1S1	1622	119	3.32
	2S6	1622	131	4.72
S11	1S21	1645	110	3.17
	1S22	1643	129	4.5
	2S28	1652	150	4.3
S12	2S12	1655	62.5	2.15
	1S16	1653	86.4	2.16
	1S24	1660	122	3.9
S13	2S7	1694	83.6	2.25
	2S23	1703	119.4	4.22
	1S5	1694	126.7	2.84
S14	2S14	1780	77.8	5.24
	2S13	1780	114	4.54
	1S15	1770	129	6.39
S15	2S18	1799	50.6	2.46
	2S11	1789	136	4.95
	2S19	1804	160	4.15
S16	1S8	1864	90.8	1.72
	2S9	1852	120	4.06
	2S27	1838	167	4.96

Table 11: Orthogonal arrays of density and strain rate for cancellous bones

Density Kg/m^3	Strain rate /s	Modulus GPa
800	120	0.174
800	165	0.059
800	200	0.099
800	165	0.059
885	120	0.117
885	165	0.143
885	200	0.222
885	165	0.143
1000	120	0.18
1000	165	0.228
1000	200	0.227
1000	165	0.228
1175	120	0.179
1175	165	0.249
1175	200	0.201
1175	165	0.249

Table 12: Effect of factor levels on the Young's modulus of the bone

A1	*A2*	*A3*	*A4*
0.098	0.21	0.216	0.22
B1	*B2*	*B3*	*A*-density
0.16	0.17	0.19	*B*-strain rate

Table 13: Orthogonal arrays of density and strain rate for cortical bones

Strain rate /s	Density Kg/m^3	Modulus Gpa
105	1380	3.2
105	1450	2.43
145	1560	3.3
145	1585	2.96
105	1595	4.53
105	1615	3.32
145	1645	4.3
145	1655	3.9
105	1700	4.22
105	1775	4.54
145	1795	4.143
145	1850	4.96
145	1380	2.61
145	1450	3.3
65	1560	2.2
65	1585	3.7
145	1595	3.62
145	1615	4.72
65	1645	3.17
65	1655	2.15
145	1700	2.84
145	1775	6.39
65	1795	2.46
65	1850	1.72
65	1380	2.57
65	1450	1.7
105	1560	2.93
105	1585	4.1
65	1595	1.44
65	1615	3.32
105	1645	4.5
105	1655	2.16
65	1700	2.25
65	1775	5.24
105	1795	4.95
105	1850	4.06

Table 14: Effect of factor levels on the Young's modulus of the bone

A1	*A2*	*A3*	*A4*	*A5*	*A6*	*A7*	*A8*	*A9*	*A10*	*A11*	*A12*
2.79	2.48	2.81	3.59	3.20	3.79	3.99	2.74	3.10	5.39	3.85	3.58
B1	*B2*	*B3*	*A*-Density in Kg/m^3								
2.66	3.75	3.92	*B*-Strain rate /s								